Computational Study on the Charge Transport and Optical Spectra of Anthracene Derivatives in Aggregates

Yajing Sun,[a] Hua Geng,[b] Qian Peng,[c] and Zhigang Shuai*[d]

A recent experiment [*Angew. Chem. Int. Ed.* **2017**, *56*, 722–727] found that a (1:9) blend film of two anthracene derivatives, 2-fluorenyl-2-anthracene (**FlAnt**) and 2-anthryl-2-anthracence (**2A**), exhibit both efficient white light emission and high hole mobility, thus promising for organic light-emitting transistors (OLETs). Employing quantum chemistry at the polarizable continuum model (PCM) and the quantum mechanics/molecular mechanics (QM/MM) levels, we investigated the excited-state structures, optical spectra, band structure and the carrier mobility for **FlAnt** and **2A** from solution to aggregate phases. We suggest using the ratio of intermolecular excitonic coupling J and intramolecular excited state relaxation energy E to judge the bathochromic shift in optical emission in aggregates. For **FlAnt**, $\rho = J/E$ is calculated to be less than 0.17, a critical value

we identified earlier, and the spectra in solution and aggregate phases present quite similar features (blue emission). However, ρ is ~0.5 for **2A** systems, and the calculated emission in the aggregate phase exhibits a remarkable bathochromic shift. In addition, the 0–0 emission is strongly suppressed in the herringbone stacking. These observations justify the experimental findings that (i) **2A** is blue emissive in solution but yellow-green in the aggregate phase, whereas **FlAnt** is always blue, and (ii) the blend of them show white emission. By using the "quantum nuclear tunneling" model we proposed earlier, we found the hole mobility for **FlAnt** and **2A** are 0.5 and 4.2 $\mathrm{cm^2\,V^{-1}\,s^{-1}}$, respectively, indicating both are good hole transport materials.

1. Introduction

Because of the potential applications in lighting and display devices, considerable attention has been paid to develop organic white-light emission materials.[1] White-light emission require materials emit light covering the entire visible spectrum, for example, with complementary-color luminescent groups.[1d,2] While linking different chemical light-emitting fragments directly often lead the spectrum shift significantly, deviating from the expected white-light, which may caused by intramolecular Förster resonance energy transfer (FRET) or other photophysical process.[3] Mixing different components to achieve white-light emission is a facile route.[4] However, physical blends tend to cause problems in instability of color, due to the discrepancies of luminescent decay rate among different components.[5] Anthracene is a widely used fluorescent material with considerable charge mobility. In the past years, it has been used in

organic effect transistor (OFET), organic light emitting diode (OLED) and other organic photoelectric devices.[6] Benifiting from its strong modifiability, anthracene derivatives were also synthesized and played important roles in the fields of photochemistry, supramolecular chemistry, photobiology and so on.[6e,7] In 2017, it was found that the mixture of **FlAnt**, a newly synthesized anthracene derivative and its by-product **2A** exhibited surprisingly white-light photoluminescence.[1f] And, the blend also exhibited high charge mobility. This is unusual because in general, the tightly packed structures with high carrier mobility would lead to enhanced non-radiative recombination, quenching luminescence: the classical Langevin's bimolecular recombination rate was simply expressed as $k = \frac{q}{\varepsilon}(\mu_e + \mu_h)$.[8] And such blend could serve as potential component for organic light-emitting transistors (OLETs), which is gaining fast-growing interests.[9]

From experiment, it was found that for **2A**, the emissions are quite different in solution and solid phases, namely, blue-emission in solution, and a significantly red-shifted yellow-green emission in solid phase. But **FlAnt** molecule exhibits blue-light emission in both solution and solid states. **2A** and **FlAnt** are both derivatives of anthracenes with quite similar molecular structure and optical emission spectra in solution. It is intriguing that these compounds demonstrated quite different luminescent behaviors in aggregates. In addition to the energy level shift in aggregate, there are two more effects on the emission spectrum: (i) suppression of 0–0 transition due to the H-aggregate symmetry cancellation;[10] (ii) and the competition between intermolecular excitonic coupling (J) and intramolecular vibrational relaxation (E), for which Li et al. have proposed to judge the spectrum shift according to the value of $\rho = J/E$: if ρ is less than the critical value 0.17, there would hardly be any

[a] Y. Sun
Department of Chemistry
Tianjin University
Tianjin 300072, PR China
[b] H. Geng
Department of Chemistry
Capital Normal University
Beijing 100048, PR China
[c] Q. Peng
Key Laboratory of Organic Solids and
Beijing National Laboratory for Molecular Science
Institute of Chemistry, Chinese Academy of Sciences
Beijing 100190, PR China
[d] Prof. Z. Shuai
MOE Key Laboratory of Organic Optoelectronics and
Molecular Engineering, Department of Chemistry
Tsinghua University, Beijing 100084, PR China
E-mail: zgshuai@tsinghua.edu.cn

bathochromic shift, as in most of the AIE (aggregation induced emission) systems; otherwise, there exist remarkable shift in emission.[11] In this work, we employ (time-dependent) density functional theory at the PCM and QM/MM levels to calculate the excited state electronic structures and band structures, optical spectra for **2A** and **FlAnt** in solution and aggregate phases, including intermolecular coupling and intramolecular excited state reorganization energy, as well as the hole mobility for crystalline phase. Both the carrier mobility and optical spectra are calculated by the MOMAP program package developed by our group (see experimental section). Our computational work can rationalize the experimental results and reveal the molecular mechanism behind the intriguing optoelectronic properties for the blend of anthracene derivatives.

2. Results and Discussion

2.1. Optimized Geometry Structure in Solution and Solid Phase

We firstly optimized the geometric structures of the two molecules, **FlAnt** and **2A**, in both solution and their solid phases. For the case of solution, we use PCM model to simulate the condition of tetrahydrofuran (THF) solvation. And for the solid phase, we use QM/MM method. We chose a supercell containing 65 molecules, and selected the central one for quantum mechanics calculation and the rest with classical mechanics modeled by UFF force field to perform the molecular mechanics calculations. Due to the extremely similar molecular structure, shown in Figure 1, **2A** and **FlAnt** possess nearly the same unit cell structure and aggregate form. Mixing of a small number of **FlAnt** molecules has little effect on the aggregation type of **2A** in the solid phase, hardly affecting the transport properties.[12] The aggregated QM/MM models we used for solid phase were shown in Figure 1c,d and based on these models, we will discuss their optical and charge transport properties separately.

For **FlAnt** molecule, the anthracene ring connected the fluorenyl ring at position 2. In solution, the dihedral angle between anthracene and fluorenyl ring is 144.06°. While in the
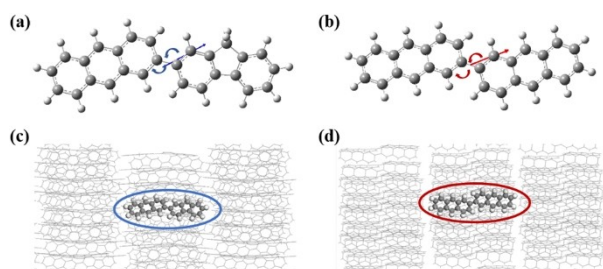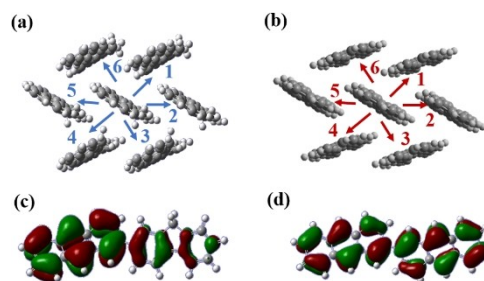
solid phase it is increased to 170.30°, owing to the compact molecular packings. Similarly, for **2A** molecule, from in solution to solid phases, the dihedral angle between the two anthracene rings is increased from 146.61° to 179.46°. These indicate that the two compounds both are close to planar structure in aggregate phase. The calculation results are really close to their single crystal structures, where the corresponding dihedral angle in **FlAnt** and **2A** are 170.06° and 179.62°, respectively.[1f] And the aggregation has a negligible effect on the bond length in both system. The calculated energies of the two moleculars in solution and aggregation are listed in Table 1.

2.2. Charge Transport Properties in Solid State

In the solid phase, the stacking structures of **FlAnt** and **2A** molecules are shown in Figure 2a and 2b. Since the interlayer coupling is very weak, we only consider the herringbone packing layer. There are six nearest neighbors around the central molecule. The distances between different molecule pairs are listed in Table 2. **2A** molecules have smaller intermolecular distances, which are 0.33Å shorter than in corresponding **FlAnt** molecule dimer, on average. The nearly planar structure of **2A** molecule contributes to more effective overlap between molecule pairs, leading much larger transfer integrals. The largest charge transfer integral is 49.20 meV, and all the hole transfer integrals are listed in Table 2. It is well known that larger transfer integrals often imply better charge transport properties. However, in case of **FlAnt**, the fluorenyl ring contains a sp^3-C atom, leading to larger steric hindrance, and the twisted structure enlarges the distance between the molecular pairs. At the same time, due to the lower symmetry of **FlAnt**, it is difficult to obtain effective overlap among the

Table 1. The B3LYP/6-31g* calculated HOMOs, LUMOs, the adiabatic excitation energy ΔE_{ad}, and vertical excitation energy ΔE_{ver} of **FlAnt** and **2A** in solution and solid phase.

	FlAnt		2A	
	Solution	Solid	Solution	Solid
HOMO [eV]	−5.238	−5.088	−5.191	−5.102
LUMO [eV]	−1.837	−1.774	−1.965	−1.919
ΔE_{ad} [eV]	2.795	2.867	2.717	2.833
ΔE_{ver} [eV]	3.013	3.043	2.868	2.959

Figure 1. The geometric structure of **FlAnt** (a) and **2A** molecular (b). Arrows indicate the direction of the transition dipole moment; The QM/MM model for **FlAnt** (c) and **2A** (d). The circled single molecules are treated as the high layer with quantum mechanical calculations, while the surrounding molecules are regarded as the low layer with molecular mechanics calculations.

Figure 2. The herringbone layer packing structures of **FlAnt** (a) and **2A** (b) single crystals with only nearest molecular pairs are numbered. Corresponding Contour plots of molecular orbitals are shown in (c) and (d).

Table 2. Center-to-center dimer separation d (Å) and its charge (hole) transfer integral V_h (in meV) of **FlAnt** and **2A**. λ (in meV) and μ [in cm^2/(Vs)] are the (intra)molecular charge reorganization energy and hole mobility, respectively.
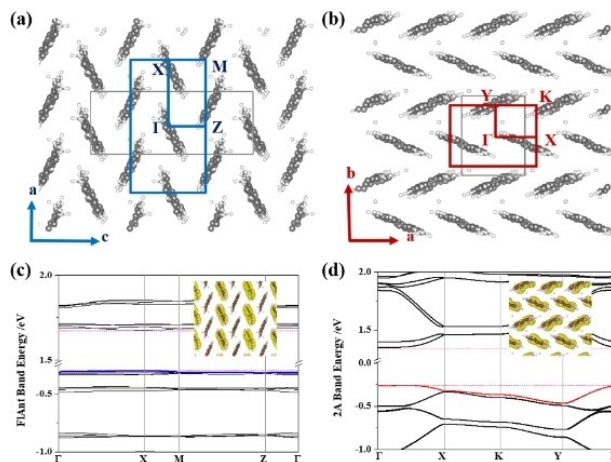
Dimer No.	FlAnt d [Å]	V_h [meV]	2A d [A]	V_h [meV]
1	5.67	6.5	4.75	49.2
2	6.05	3.5	5.96	28.2
3	5.01	56.5	4.78	35.8
4	5.09	19.5	4.81	41.6
5	6.05	3.5	5.96	28.2
6	5.14	13.2	4.78	41.8
λ [meV]	146		108	
μ [cm^2/(Vs)]	$\mu\_a = 0.20$		$\mu\_a = 4.17$	
	$\mu\_c = 0.51$		$\mu\_b = 3.46$	

Figure 3. The first Brillouin zones (a) and (b) and band structures (c) and (d) along high-symmetry direction of **FlAnt** and **2A** single crystal. The colored bands are the valence band of **FlAnt** (blue) and **2A** (red), respectively. The insets are the charge density distributions of valence band.

adjacent molecular orbitals. In Figure 2c, there is a significant difference in molecular orbital (MO) distribution of anthracene and fluorenyl rings. If two **FlAnt** molecules in the molecule pair are opposite, MO of the adjacent anthracene and fluorenyl ring cannot overlap effectively, which will hinder the charge transport. Only if two anthracene rings adjacent to each other, the hopping paths has a certain charge transfer integral, that is, the 3rd-dimer with V_h of 56.50 meV.
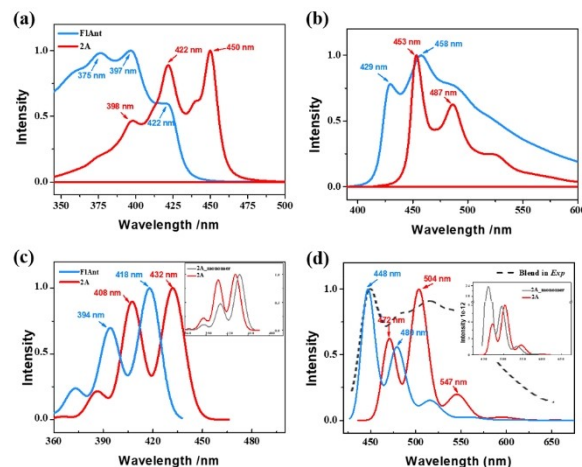
We employ the "quantum nuclear tunneling model" to calculate the hole mobility. Since the LUMO level is about −2 eV, much higher than the required −3.5 to −4 eV level for electron injection, so both **2A** and **FlAnt** are hole transport materials. We calculate only the hole mobility. For **2A**, the hole mobilities along two perpendicular crystal axis directions a- and b-directions are calculated to be 4.17 and 3.46 cm^2/Vs, respectively. For **FlAnt**, the mobilities are 0.20 and 0.51 cm^2/Vs along the two orthogonal crystal axis directions. The rigid structure of **2A** implies a smaller reorganization energy, favorable to charge transport. The reorganization energy of **2A** is 108 meV, around 40 meV smaller than that of **FlAnt**. The difference in mobility can be partly attributed to the reorganization energy. And it is also helpful to refer to the band structures (Figure 3). The valence band width of **FlAnt** is calculated to be only 17.33 meV and the average effective hole mass is as large as 3.15 m$_e$. But the bandwidth of **2A** is 207 meV, more than 10 times larger than that of **FlAnt**. As a results, **2A** crystal has smaller effective mass, only 0.42 m$_e$.

Figure 4. The calculated absorption (a) and emission (b) spectra of **FlAnt** and **2A** in THF solution. Blue and red lines refer to **FlAnt** and **2A**, respectively. Calculated absorption (c) and emission (d) spectra in the solid state. The insets show the influence of aggregation effect of **2A**. The red and gray lines refer to the spectra of **2A** with and without considering exciton coupling. The experimental emission of the **FlAnt**:**2A** blend is sketched as a dashed guideline in (d) for comparison.

2.3. Optical Properties in Solution and Solid Phase

We then calculated the photophysical properties of the two anthracene derivatives in solution. In Figure 4a, we found that **FlAnt** mainly absorbs the light with wavelength of 375–422 nm in solution. And the absorption wavelength of **2A** molecule is 398–450 nm, slightly red-shifted from that of **FlAnt**. From the calculated emission spectra, we found both of the two molecules mainly emit blue light with the maximum peak of around 455 nm in solution, Figure 4b. Our calculated results are consistent well with the blue-light emission observed in the experiments.[1f]

Furthermore, we calculated the optical properties of the two molecules in their solid state. As known, the molecular aggregates always have different luminescent properties with the monomers due to intermolecular interactions, including electrostatic interaction, Van der Waals interaction and excitonic interaction and so forth.[10b,13] The first two kind of interactions can be fully considered by QM/MM approach. For the latter, the Frenkel exciton model is usually adopted, and there are two types, J-type and H-type aggregation, according to the arrangement of transition dipole moments in molecular aggregates. The J-type aggregation is head-to-tail arrangement and it can enhance the intensity of absorption and emission spectra. While the H-type aggregation is side-by-side, and it can weaken the

ChemPhysChem

Articles
doi.org/10.1002/cphc.202000187

Chemistry Europe
European Chemical
Societies Publishing

luminescence intensity compared with those of the single molecule.[10a,14] In 2017, a criterion, the ratio of intermolecular excitonic coupling and intramolecular vibrational relaxation ($\rho = J/E$), was proposed to judge the effect of the exciton coupling on the optical spectra. They suggested when ρ is larger than 0.17 at room temperature, the aggregated optical spectra would be obviously changed, deviating from the luminescence properties of single molecule.[15]

Following the suggestion, we firstly calculated the E and J of the six nearest molecule pairs and listed J and their ratio $\rho = J/E$ in Table 3. For **FlAnt** molecular, all the J values are small (10~28 meV) while the E is much larger (171 meV), resulting in $\rho \sim 0.1$, less than the critical value of 0.17 we identified earlier.[9] It implies the excitonic interaction would have very little influence on the optical spectra. With the help of QM/MM method coupled with the finite temperature Franck-Condon vibration resolved spectrum formalism, we first calculated the absorption and emission spectra of **FlAnt** in aggregate state considering the intermolecular electrostatic and Van der Waals interaction. There are two obvious absorption peaks at 418 nm and 394 nm. The emission spectrum has maximum peak at 448 nm. These are also in good agreement with available experimental emission spectrum of maximum peak about at 450 nm in **FlAnt** thin film.[1f] Due to the weak excitonic interaction, the aggregated **FlAnt** maintain the same blue-light emission as they are in solution. But for **2A**, the reorganization energy of the excited state is calculated to be 123 meV, much less than that of **FlAnt**. Meantime, the excitonic coupling strengths are much larger, reaching 66.3 meV. The ρ values are calculated to be as high as 0.5, much larger than the critical value 0.17. These suggest the excitonic coupling would obviously quench the 0–0 emission peak and generate a red shifted enhanced 0–1 emission peak, leading to remarkable bathochromic shift in solid from solution. As expected, in the calculated emission spectrum, Figure 4d, the blue 0–0 emission peak is suppressed greatly, and a yellow-green peak appears, which are consistent with the observed light near 470–550 nm in the experiment.[1f] Additionally, there is an obvious energy gap (432 vs. 472 nm) between the absorption and emission peak. We can reasonably rule out the possibility of reabsorption. Therefore, it is verified by our calculation that blue **FlAnt** and yellow-green **2A** blend could exhibit white-light emission in a specific proportion. Last, it should be pointed out that the critical value 0.17 was obtained in an empirical way, namely,

derived from theoretical calculation and the experimental results for quite a lot of molecules.[9]

It is thus expected that in the blend of **2A** and **FlAnt**, due to the well shifted emission of **2A**, none of the emission could be re-absorbed, forming a complimentary emission spectrum (Figure 4d), giving rise to a white color.

3. Conclusions

In conclusion, we have elucidated the molecular mechanism for the white-light emission and high-mobility of the blend of anthracene derivatives blend **2A** and **FlAnt**, implying possible application in OLETs. For **2A** in solid phase, the strong excitonic coupling with a $\rho = J/E$ value typically around 0.5, induces a notable red-shift 0–1 yellow-green emission spectrum, largely suppressing the 0–0 emission, leading to a remarkable bathochromic shift. And **FlAnt** in the solid phase with a small ρ value (less than 0.17) maintains the blue-light with negligible excitonic coupling effect. Therefore, mixed with a small amount of blue-emitting **FlAnt** molecules, the **2A** aggregates exhibit white-light emission. At the same time, the blend still maintains high mobility owing to the closed packed structure of anthracene derivatives, which indicates the promising application in organic white-light-emitting transistors. The calculated carrier mobility based on quantum nucleatr tunneling model and the effective mass based on band structure indicate the two anthracene derivatives are good hole transport materials. Mixing a small amount of heterochromatic molecules with the same aggregation and very similar geometry can effectively regulate the luminescent properties and maintain the charge transfer performance simultaneously. Following the above strategy, we propose that color-controlled materials may be realized by mixing high mobility organic molecules with similar structure. Our work can well explain the white-light emission of anthracene derivatives blend and provides theoretical guidance for design white-light emitting materials with high mobility.

Experimental Section

Charge Transfer Properties

When calculating the charge mobilities, we use the hopping model considering nuclear tunneling effect.[16] In this model, every hopping event can be regarded as a non-adiabatic charge transfer process. Under the perturbation theory and the displacement harmonic oscillator approximation, the charge transfer rate k_{fi} can be derived from Fermi's Golden Rule [Eq. (1)]:

$$k_{fi} = \frac{|V_{fi}|^2}{\hbar^2} \int_{-\infty}^{\infty} dt$$
$$exp\left\{ it\omega_{fi} - \sum_j S_j \left[(2n_j + 1) - n_j e^{-it\omega_j} (n_j + 1) e^{it\omega_j} \right] \right\} \quad (1)$$

Where V_{fi} is the transition integral between the initial and final states. S_j is Huang-Rhys factor of the normal vibration mode j,

Table 3. The exciton coupling strength J (in meV) in aggregation and its ratio with the excited state intramolecular vibrational relaxation energy E (in meV), $\rho = J/E$ for **FlAnt** and **2A**.

| Dimer No. | FlAnt | | 2A | |
	J	ρ	J	ρ
1	27	0.15	66	0.54
2	12	0.07	20	0.16
3	10	0.06	66	0.54
4	15	0.06	30	0.24
5	12	0.07	20	0.16
6	28	0.16	24	0.19
E	171		123	

ChemPhysChem

Articles
doi.org/10.1002/cphc.202000187

Chemistry Europe
European Chemical
Societies Publishing

measuring the strength of electron-phonon coupling, $S_j = \lambda_j/\hbar\omega_j$. λ_j, ω_j are the reorganization energy and vibration frequency of the jth normal mode. And n_j is the distribution of phonon occupancies, $n_j = 1/[\exp\left(\frac{\hbar\omega_j}{k_BT}\right) - 1]$. In the hopping model, the charge mobility can be expressed as [Eq. (2)]:

$$\mu = \frac{e}{k_BT}D \tag{2}$$

D is diffusion coefficient, calculated by dynamic Monte Carlo simulation.[17] $D = \frac{1}{2n}\lim_{t\to\infty}\frac{\langle r^2 \rangle}{t}$, in which r is the displacement of charge carrier. When performing dynamic simulation, we choose one molecule as the initial charge site, and assume the charge can only transit to the nearest neighboring molecule. The hopping probability of charge between nearest molecules pair is $P_\alpha = \frac{k_{mn}}{\sum_{n'} k_{mn'}}$, where k_{mn} is the hopping rate of charge from molecule m to n, and n' represents all the nearest neighbors. So, the residence time of charge carrier at m can be expressed as $\frac{1}{\sum_{n'} k_{mn'}}$. After Monte Carlo simulation, we find out the linear relationship between the mean square displacement and simulation time, getting the diffusion coefficient and charge mobilities.

We optimized the geometric structure and calculated the properties of neutral and charged molecules using Gaussian 16 package.[18] The vibration information and charge transfer integrals between molecular pairs are performed at the *ab initio* density functional theory calculation with B3LYP function and 6-31G* basis set.[19] The Huang-Rhys factors S_j and the reorganization energy λ_j of each vibration mode are obtained with the help of DUSHIN program.[20] The MOMAP[21] package is used to calculate the remaining charge transfer properties. Meanwhile, the electronic band structure was calculated by the Vienna Ab Initio Simulation Package (VASP)[22] using projector-augmented wave (PAW) method and the exchange correlation interactions was described by generalized gradient approximation (GGA).[23] Base on electronic band structure, we also get the charge effective mass of the two molecular crystals.

Optical Properties

We calculated the absorption and emission spectra of **FlAnt** and **2 A** molecule in solution and solid phases. According to the Fermi Golden rule and Franck - Condon principle,[24] the molecular absorption σ_{ab} [Eq. (3)] and emission spectra σ_{em} [Eq. (4)] are written as:[1,9,24c]

$$\sigma_{ab}(\omega, T) = \frac{4\pi^2\omega}{3\hbar c}|\mu_{fi}|^2 \sum_{u,\nu} P_{i\nu}|\langle\Theta_{fu}|\Theta_{i\nu}\rangle|^2\delta(\omega - \omega_{fu,i\nu}) \tag{3}$$

$$\sigma_{em}(\omega, T) = \frac{4\omega^3}{3\hbar c^3}|\mu_{fi}|^2 \sum_{u,\nu} P_{i\nu}|\langle\Theta_{fu}|\Theta_{i\nu}\rangle|^2\delta(\omega_{i\nu,fu} - \omega) \tag{4}$$

here, $\hbar$ is the Planck constant. c is the speed of light. $P_{i\nu}$ is the Boltzmann distribution function of the initial vibration at finite temperature. Θ is the wave function of nuclear vibration between different initial and final states with vibrational quantum number of ν and u. And μ_{fi} is the electric transition dipole moment between states $|\Phi_i\rangle$ and $|\Phi_f\rangle$. For the solid phase, vibronic coupled exciton model was used to construct the excion Hamiltonian. For simplicity, we consider only a dimer system and the Hamiltonian matrix can be expressed as:[11]

$$H_e = \begin{pmatrix} 1/2\hbar\omega + \varepsilon & 0 & J\xi_{0-0}\xi_{0-0} & J\xi_{1-0}\xi_{0-0} \\ 0 & 3/2\hbar\omega + \varepsilon & J\xi_{0-0}\xi_{0-1} & J\xi_{1-0}\xi_{0-1} \\ J\xi_{0-0}\xi_{0-0} & J\xi_{0-0}\xi_{0-1} & 1/2\hbar\omega + \varepsilon & 0 \\ J\xi_{1-0}\xi_{0-0} & J\xi_{1-0}\xi_{0-1} & 0 & 3/2\hbar\omega + \varepsilon \end{pmatrix} \tag{5}$$

$\xi_{0-\nu}$ is the Franck-Condon integration between ground state with quantum number 0 and excited state with ν. The eigenvalue and eigenvector of the excited states can be obtained by diagonalizing Equation (5), from which we can get the absorption and emission spectra based on Equations (3) and (4).

The optical spectra were simulated by the MOMAP program coupled with Gaussian 16.[18] Based on PCM model, we optimized and calculated the ground and excited station properties of the two molecules in tetrahydrofuran solution at (TD)B3LYP/6-31G* level.[25] And when describing them in solid phase, ONIOM model is used.[26] We constructed supercell based on the experimental crystal structure. The central molecule was calculated by quantum mechanical method with (TD)B3LYP/6-31G*, and the surrounding molecules are regarded as the lower layer calculated using molecular mechanics in UFF force field. Electrostatic embedding is implied to describe the electrostatic interaction between organic molecules.[26f] To simplify the calculation, we keep those vibrational modes with Franck-Condon overlap integral more than 1% kept in Equations (3) and (4), which is 11 modes, enough for convergence. We found that the calculated spectra for the six dimers are very similar. So we just present results from one dimer with the largest J in Figure 4.

Conflict of Interest

The authors declare no conflict of interest.

[1] a) J. Kido, M. Kimura, K. Nagai, *Science* **1995**, *267*, 1332–1334; b) S. Reineke, F. Lindner, G. Schwartz, N. Seidler, K. Walzer, B. Lussem, K. Leo, *Nature* **2009**, *459*, 234–238; c) M. C. Gather, A. Köhnen, A. Falcou, H. Becker, K. Meerholz, *Adv. Funct. Mater.* **2007**, *17*, 191–200; d) G. M. Farinola, R. Ragni, *Chem. Soc. Rev.* **2011**, *40*, 3467–3482; e) C. Vijayakumar, V. K. Praveen, A. Ajayaghosh, *Adv. Mater.* **2009**, *21*, 2059–2063; f) M. Chen, Y. Zhao, L. Yan, S. Yang, Y. Zhu, I. Murtaza, G. He, H. Meng, W. Huang, *Angew. Chem.* **2017**, *56*, 722–727; g) S. S. Babu, J. Aimi, H. Ozawa, N. Shirahata, A. Saeki, S. Seki, A. Ajayaghosh, H. Mohwald, T. Nakanishi, *Angew. Chem.* **2012**, *51*, 3391–3395; h) K. T. Kamtekar, A. P. Monkman, M. R. Bryce, *Adv. Mater.* **2010**, *22*, 572–582; i) N. J. Findlay, J.

ChemPhysChem

Articles
doi.org/10.1002/cphc.202000187

**Chemistry
Europe**
European Chemical
Societies Publishing

Bruckbauer, A. R. Inigo, B. Breig, S. Arumugam, D. J. Wallis, R. W. Martin, P. J. Skabara, *Adv. Mater.* **2014**, *26*, 7290–7294.

[2] a) Z. Xie, C. Chen, S. Xu, J. Li, Y. Zhang, S. Liu, J. Xu, Z. Chi, *Angew. Chem.* **2015**, *54*, 7181–7184; b) Q. Y. Yang, J. M. Lehn, *Angew. Chem.* **2014**, *53*, 4572–4577.

[3] a) J. V. Caspar, T. J. Meyer, *J. Phys. Chem.* **1983**, *87*, 952–957; b) J. V. Caspar, E. M. Kober, B. P. Sullivan, T. J. Meyer, *J. Am. Chem. Soc.* **1982**, *104,*, 630–632; c) J. Liang, B. Z. Tang, B. Liu, *Chem. Soc. Rev.* **2015**, *44*, 2798–2811; d) J. Mei, Y. Hong, J. W. Lam, A. Qin, Y. Tang, B. Z. Tang, *Adv. Mater.* **2014**, *26*, 5429–5479.

[4] a) L. Ying, C. L. Ho, H. Wu, Y. Cao, W. Y. Wong, *Adv. Mater.* **2014**, *26*, 2459–2473; b) G. Zhou, Q. Wang, X. Wang, C. L. Ho, W. Y. Wong, D. Ma, L. Wang, Z. Lin, *J. Mater. Chem. C* **2010**, *20*, 7472.

[5] a) R. Wang, D. Liu, H. Ren, T. Zhang, H. Yin, G. Liu, J. Li, *Adv. Mater.* **2011**, *23*, 2823–2827; b) H. Wei, Z. Zhao, C. Wei, G. Yu, Z. Liu, B. Zhang, J. Bian, Z. Bian, C. Huang, *Adv. Funct. Mater.* **2016**, *26*, 2085–2096; c) Q. W. Zhang, D. Li, X. Li, P. B. White, J. Mecinovic, X. Ma, H. Agren, R. J. M. Nolte, H. Tian, *J. Am. Chem. Soc.* **2016**, *138*, 13541–13550.

[6] a) J. Van Damme, F. Du Prez, *Prog. Polym. Sci.* **2018**, *82*, 92–119; b) M. Pope, H. P. Kallmann, P. Magnante, *J. Chem. Phys.* **1963**, *38*, 2042–2043; c) M.-H. Ho, B. Balaganesan, C. H. F. Chen, *Isr. J. Chem.* **2012**, *52*, 484–495; d) A. I. Korn, R. A. Arnst, A. C. Damask, *Phys. Rev.* **1969**, *186*, 3; e) M. Chen, L. Yan, Y. Zhao, I. Murtaza, H. Meng, W. Huang, *J. Mater. Chem. C* **2018**, *6*, 7416–7444.

[7] a) J. Liu, H. Zhang, H. Dong, L. Meng, L. Jiang, L. Jiang, Y. Wang, J. Yu, Y. Sun, W. Hu, A. J. Heeger, *Nat. Commun.* **2015**, *6*, 10032; b) M. Yoshizawa, J. K. Klosterman, *Chem. Soc. Rev.* **2014**, *43*, 1885–1898; c) J. Li, K. Zhou, J. Liu, Y. Zhen, L. Liu, J. Zhang, H. Dong, X. Zhang, L. Jiang, W. Hu, *J. Am. Chem. Soc.* **2017**, *139*, 17261–17264; d) H. Meng, F. Sun, M. B. Goldfinger, G. D. Jaycox, Z. Li, W. J. Marshall, G. S. Blackman, *J. Am. Chem. Soc.* **2005**, *127*, 2406–2407; e) A. Dadvand, A. G. Moiseev, K. Sawabe, W. H. Sun, B. Djukic, I. Chung, T. Takenobu, F. Rosei, D. F. Perepichka, *Angew. Chem.* **2012**, *51*, 3837–3841.

[8] P. Langevin, *Ann. Chim. Phys.* **1903**, *28,*, 433.

[9] a) F. Cicoira, C. Santato, *Adv. Funct. Mater.* **2007**, *17*, 3421–3434; b) A. Hepp, H. Heil, W. Weise, M. Ahles, R. Schmechel, H. von Seggern, *Phys. Rev. Lett.* **2003**, *91*, 157406; c) S. Hotta, T. Yamao, S. Z. Bisri, T. Takenobu, Y. Iwasa, *J. Mater. Chem. C* **2014**, *2*, 965–980; d) L. Xie, W. Li, W. Huang, M. Yi, N. Zhang, W. Bian, *Chin. Sci. Bull.* **2013**, *58*, 1817–1832.

[10] a) F. C. Spano, *Acc. Chem. Res.* **2010** *43*, 429–439; b) F. C. Spano, *Annu. Rev. Phys. Chem.* **2006**, *57*, 217–243.

[11] W. Li, Q. Peng, Y. Xie, T. Zhang, Z. Shuai, *Acta Chim. Sin.* **2016**, *74*, 902.

[12] T. Liu, Y. Guo, Y. Yi, L. Huo, X. Xue, X. Sun, H. Fu, W. Xiong, D. Meng, Z. Wang, F. Liu, T. P. Russell, Y. Sun, *Adv. Mater.* **2016**, *28*, 10008–10015.

[13] J. Gierschner, L. Lüer, B. Milián-Medina, D. Oelkrug, H. Egelhaaf, *J. Phys. Chem. Lett.* **2013**, *4*, 2686–2697.

[14] a) M. Kasha, *Radiat. Res.* **1963**, *20*, 55–71; b) M. Kasha, H. Rawls, M. A. El-Bayoumi, *Pure Appl. Chem.* **1965**, *11*, 371–392; c) F. C. Spano, L. Silvestri, *J. Chem. Phys.* **2010**, *132*, 094704.

[15] a) J. Frenkel, *Phys. Rev.* **1931**, *37*, 17–44; b) W. Li, Q. Peng, H. Ma, J. Wen, J. Ma, L. A. Peteanu, Z. Shuai, *Chem. Mater.* **2017**, *29*, 2513–2520.

[16] a) G. Nan, X. Yang, L. Wang, Z. Shuai, Y. Zhao, *Phys. Rev. B* **2009**, *79*; b) L. Wang, Q. Li, Z. Shuai, L. Chen, Q. Shi, *Phys. Chem. Chem. Phys.* **2010**, *12*, 3309–3314; c) H. Geng, Q. Peng, L. Wang, H. Li, Y. Liao, Z. Ma, Z. Shuai, *Adv. Mater.* **2012**, *24*, 3568–3572.

[17] Z. Shuai, H. Geng, W. Xu, Y. Liao, J. M. Andre, *Chem. Soc. Rev.* **2014**, *43*, 2662–2679.

[18] Gaussian 16 (Revision A. 03##), M. J. Frisch, G. W. Trucks, H. B. Schlegel, G. E. Scuseria, M. A. Robb, J. R. Cheeseman, G. Scalmani, V. Barone, G. A. Petersson, H. Nakatsuji, X. Li, M. Caricato, A. V. Marenich, J. Bloino, B. G. Janesko, R. Gomperts, B. Mennucci, H. P. Hratchian, J. V. Ortiz, A. F. Izmaylov, J. L. Sonnenberg, Williams, F. Ding, F. Lipparini, F. Egidi, J. Goings, B. Peng, A. Petrone, T. Henderson, D. Ranasinghe, V. G. Zakrzewski, J. Gao, N. Rega, G. Zheng, W. Liang, M. Hada, M. Ehara, K. Toyota, R. Fukuda, J. Hasegawa, M. Ishida, T. Nakajima, Y. Honda, O. Kitao, H. Nakai, T. Vreven, K. Throssell, J. A. Montgomery Jr., J. E. Peralta, F. Ogliaro, M. J. Bearpark, J. J. Heyd, E. N. Brothers, K. N. Kudin, V. N. Staroverov, T. A. Keith, R. Kobayashi, J. Normand, K. Raghavachari, A. P. Rendell, J. C. Burant, S. S. Iyengar, J. Tomasi, M. Cossi, J. M. Millam, M. Klene, C. Adamo, R. Cammi, J. W. Ochterski, R. L. Martin, K. Morokuma, O. Farkas, J. B. Foresman, D. J. Fox, Wallingford, CT, **2016**..

[19] a) C. Lee, W. Yang, R. G. Parr, *Phys. Rev. B* **1988**, *37*, 785–789; b) A. D. Becke, *J. Chem. Phys.* **1993**, *98,*, 5648; c) A. D. Becke, *Phys. Rev. A* **1988**, *38*, 3098–3100.

[20] J. R. Reimers, *J. Chem. Phys.* **2001**, *115*, 9103–9109.

[21] Y. Niu, W. Li, Q. Peng, H. Geng, Y. Yi, L. Wang, G. Nan, D. Wang, Z. Shuai, *Mol. Phys.* **2018**, *116*, 1078–1090.

[22] a) G. Kresse, J. Furthmuller, *Phys. Rev. B* **1996**, *54* 11169–11186; b) G. Kresse, J. Furthmiiller, *Comput. Mater. Sci.* **1996**, *6* 15–50.

[23] J. P. Perdew, K. Burke, M. Ernzerhof, *Phys. Rev. Lett.* **1996**, *77*, 3865–3868.

[24] a) E. U. Condon, *Phys. Rev.* **1928**, *32*, 858–872; b) J. Franck, E. G. Dymond, *Trans. Faraday Soc.* **1926**, *21*, 536–542; c) S. H. Lin, C. H. Chang, K. K. Liang, R. Chang, Y. J. Shiu, J. M. Zhang, T. S. Yang, M. Hayashi, F. C. Hsu, *Adv. Chem. Phys.* **2002**, 1–88.

[25] J. Tomasi, B. Mennucci, R. Cammi, *Chem. Rev.* **2005**, *105*, 2999–3094.

[26] a) A. Warshel, M. Karplus, *J. Am. Chem. Soc.* **1972**, *94*, 5612–5625; b) A. Warshel, M. Levitt, *J. Mol. Biol.* **1976**, *103*, 227–249; c) J. To, P. Sherwood, A. A. Sokol, I. J. Bush, C. R. A. Catlow, H. J. J. van Dam, S. A. French, M. F. Guest, *J. Mater. Chem.* **2006**, *16*, 1919; d) H. M. Senn, W. Thiel, *Curr. Opin. Chem. Biol.* **2007**, *11*, 182–187; e) G. Groenhof, *Angew. Chem.* **2013**, *52*, 12489–12491; f) D. Bakowies, W. Thiel, *J. Phys. Chem.* **1996**, *100*, 10580–10594.

ARTICLES

Shining white! We have thoroughly investigated the internal cause of the white light emission and high mobility of anthracene-derivative blend. The dense aggregation structure of **2 A** molecule plays the key role in the extraordinary photo-electric property. We proposed the color control may be realized by mixing homomorphic derivatives in organic photoelectric material engineering.
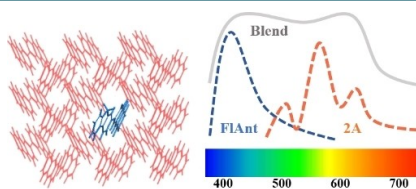
Y. Sun, H. Geng, Q. Peng, Prof. Z. Shuai*

1 – 7

Computational Study on the Charge Transport and Optical Spectra of Anthracene Derivatives in Aggregates